RSC Advances

PAPER

View Article Online
View Journal | View Issue

Cite this: *RSC Adv.*, 2022, **12**, 10401

A facile chemical synthesis of nanoflake NiS_2 layers and their photocatalytic activity

Mohammed M. Gomaa, *[a] Mohamed H. Sayed, [ab] Mahmoud S. Abdel-Wahed [c] and Mostafa Boshta[a]

A single-phase and crystalline NiS_2 nanoflake layer was produced by a facile and novel approach consisting of a two-step growth process. First, a $Ni(OH)_2$ layer was synthesized by a chemical bath deposition approach using a nickel precursor and ammonia as the starting solution. In a second step, the obtained $Ni(OH)_2$ layer was transformed into a NiS_2 layer by a sulfurization process at 450 °C for 1 h. The XRD analysis showed a single-phase NiS_2 layer with no additional peaks related to any secondary phases. Raman and X-ray photoelectron spectroscopy further confirmed the formation of a single-phase NiS_2 layer. SEM revealed that the NiS_2 layer consisted of overlapping nanoflakes. The optical bandgap of the NiS_2 layer was evaluated with the Kubelka–Munk function from the diffuse reflectance spectrum (DRS) and was estimated to be around 1.19 eV, making NiS_2 suitable for the photodegradation of organic pollutants under solar light. The NiS_2 nanoflake layer showed photocatalytic activity for the degradation of phenol under solar irradiation at natural pH 6. The NiS_2 nanoflake layer exhibited good solar light photocatalytic activity in the photodegradation of phenol as a model organic pollutant.

Received 17th February 2022
Accepted 22nd March 2022

DOI: 10.1039/d2ra01067d

rsc.li/rsc-advances

Introduction

In the last decades, nanostructured transition metal sulfides (NTMSs) have received considerable attention in different fields because of their unique optical, magnetic and catalytic properties.[1–3] The properties of these materials are strongly dependent on the dimension, size, and morphologies of fabricated materials,[4–6] making these materials very promising for numerous advanced applications such as adsorbents for dye removal,[7] supercapacitors,[8] rechargeable lithium-ion batteries,[9] hydrodesulfurization catalysts,[10] hydrogen evolution reaction,[4,11,12] and catalysts in the degradation of organic dyes.[13]

Metal sulfide materials such as zinc sulfide,[14] manganese sulfide,[15] silver sulfide,[16] iron sulfide,[17] molybdenum sulfide,[18] nickel sulfide,[12] and copper sulfides, have been reported and studied extensively.[19] Among the metal sulfides, nickel sulfides are more favorable in terms of earth-abundant resources, forming numerous phases such as NiS, NiS_2, Ni_3S_2, Ni_3S_4, Ni_7S_6, and Ni_9S_8, which are suitable as alternative materials for different applications.[20–23] Nickel disulfide (NiS_2) crystallizes in a pyrite-like structure (FeS_2), with a cubic phase $Pa\bar{3}$ symmetry.[10,24,25] Nanostructured pyrite NiS_2 with a cubic structure has interesting optical, electronic, and magnetic properties.[3,10,26] NiS_2 nanostructures with controlled morphology such as nanoparticles, nanowires, nanosheets and hollow microspheres,[27–29] have been considered as promising semiconducting materials for catalytic applications due to their low-cost, nontoxicity and chemical stability.[30,31] However, the catalytic performance of NiS_2 in the degradation of organic pollutants such as endocrine disrupting compounds (EDCs) is still less competitive compared to other catalytic materials based on phosphides and noble metals.[4,13] In this regard, numerous techniques have been used to develop and fabricate nickel sulfide nanostructures with good physical and chemical properties including hydrothermal methods,[23,32,33] solvothermal,[34] decomposition of single-source precursors,[35] microwave-assisted synthesis,[36,37] solventless route in air,[38] sonochemical,[39] and ultrasonic spray pyrolysis.[10] Most of these methods are suitable for preparing nickel sulfides in powder form with other different phases sometimes accompanying.[22,29,38] The different possible phases of nickel sulfide make the synthesis of single-phase nickel disulfide very complicated.[20,29,34] Therefore, the demand for an alternative approach to prepare a single phase of nickel disulfide layers with a high specific area and uniform morphology is still a major challenge, and will open doors to various opportunities for advanced applications.

Endocrine disrupting compounds (EDCs) such as phenol and its derivatives are a category of dangerous persistent organic pollutants, which are usually present in low concentrations in water environments. Phenol molecules are considered very harmful to human health, marine creatures and living

[a]Solid State Physics Department, National Research Centre, 12622 Dokki, Giza, Egypt. E-mail: dr.metwalyg@gmail.com; Tel: +20-1272110812

[b]Molecular and Fluorescence Spectroscopy Lab., Central Laboratories Network, National Research Centre, 12622 Dokki, Giza, Egypt

[c]Water Pollution Research Department, National Research Centre, 12622 Dokki, Giza, Egypt

organisms due to their carcinogenic, mutagenic, stability, and bioaccumulation nature, even in low concentrations. Phenolic compounds are discharged to ecology through effluent from many industries for instance, paint production, processing of petroleum, tanning, and pharmaceuticals.[40–42] The conventional treatment is not very effective for the removal of these hazardous pollutants. Thus, the development of novel techniques is essential to address this issue. Morphological control is one of the effective approaches for promoting the photodegradation of phenol using NiS_2 with nanoflake morphology. One of the big problems in the photocatalyst process is separation and recovery restriction of the photocatalyst from effluent after the treatment process. Therefore, herein, this problem is overcome through immobilizing prepared nickel sulfide on a glass substrate as layers.

In this study, single-phase NiS_2 nanoflake layers were successfully processed *via* a facile two-step fabrication process. First, $Ni(OH)_2$ nanoflake layers were grown on glass substrates by the chemical bath deposition method, followed by the phase transformation of $Ni(OH)_2$ into NiS_2 *via* a sulfurization process. Structural, morphological and optical properties as well as the catalytic activity of the obtained NiS_2 layer were studied. The unique nanoflake-like morphology of NiS_2 serves as an efficient photocatalyst for the degradation of destructive organic pollutants (phenol as the model organic compound).

Experimental

NiS_2 layers deposition

First, the chemical bath deposition (CBD) approach was used for the synthesis of the nanoflake-structured nickel hydroxide layer. The glass substrates were ultrasonically cleaned using acetone and ethyl alcohol for 20 min followed by distilled water, then dried with nitrogen gas, prior to loading into the reaction bath. 0.1 M aqueous solution of nickel chloride ($NiCl_2 \cdot 6H_2O$ – Sigma Aldrich) and ammonia solution were used as the source of Ni^{2+} and complexing agent for layer deposition, respectively. In a typical experimental procedure, the ammonia solution was added drop wise into the nickel chloride solution under continuous magnetic stirring to produce a clear and homogeneous aqueous solution as the starting solution. The precleaned glass substrates were vertically immersed in the solution bath at optimum deposition temperature, (T_d = 50 °C) and pH 11 during the synthesis process. After 2 h, the blue-colored solution changed to a greenish white color with the formation of $Ni(OH)_2$ layer on the surface of the substrate by the adsorption and nucleation of the nickel cations on the substrate. The as-deposited $Ni(OH)_2$ layers were transferred into a tube furnace with excessive sulfur powder and subsequently sulfurized at 450 °C for 1 h in nitrogen atmosphere to obtain a nickel sulfide layer.[43,44] For the ease of understanding, the facile CBD and synthesis process for the nanoflake structured NiS_2 layer is schematically described in Fig. 1.

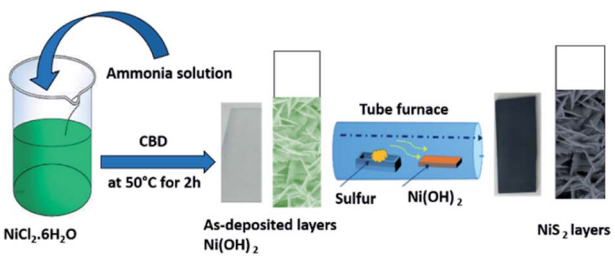

Fig. 1 Schematic description of the synthesis of porous NiS_2 nanoflake layers.

The formation mechanism of the nanoflake-structured nickel disulfide layer is divided into two processes: first, the formation of a nickel hydroxide phase *via* the chemical bath deposition route, as indicated by the following equations:

$$Ni^{2+} + 2OH^- \rightarrow Ni(OH)_2\downarrow \quad (1)$$

$$Ni(OH)_2 + 4NH_3 \rightarrow [Ni(NH_3)]^{4+} + 2OH^- \quad (2)$$

$$[Ni(NH_3)]^{4+} + 2OH^- \rightarrow Ni(OH)_2\downarrow + 4NH_3\uparrow \quad (3)$$

The detailed mechanism of the formation of nickel hydroxide by chemical bath deposition (CBD) can be found elsewhere.[45,46]

Second, the transformation of as deposited $Ni(OH)_2$ layers to nickel disulfide² due to reaction of $Ni(OH)_2$ with sulfur atoms at 450 °C according to the following reactions:

$$Ni(OH)_2 + S \leftrightarrow NiS + 2OH^- \quad (4)$$

$$NiS + S \rightarrow NiS_2 \quad (5)$$

Characterization of prepared immobilized NiS_2

In this study, the structural investigation and phase identification of the as-prepared NiS_2 layer was analyzed by X-ray powder diffraction (XRD) with a Panalytical X'Pert diffractometer using Cu Kα1 radiation at 45 kV and 40 mA. Scanning electron microscopy (SEM) (QUANTA FEG250) was used for the surface morphology imaging of the obtained layers. X-ray photoelectron spectroscopy (XPS) was collected on K-Alpha (Themo Fisher Scientific, USA) with monochromatic X-ray Al K-alpha radiation at pressure 10^{-9} mbar to determine the elemental composition and electronic states of the NiS_2 layer. Raman analysis was performed on a confocal Raman microscope model WITec Alpha 300 RA under the laser excitation of 532 nm. Diffuse reflectance spectra were carried out using a UV/Vis/NIR spectrophotometer (Jasco V770) in the wavelength range 250–1000 nm.

Evaluation of the photocatalytic performance of the as-prepared immobilized NiS_2 layer

The photocatalytic performance of the as-prepared NiS_2 layer was established by photodegradation of phenol as a model organic pollutant. For this purpose, the NiS_2 slide is primarily fixed by a silicon adhesive on a 2 cm-height edge inside a 150 mL beaker. After that, 90 mL of 10 mg L^{-1} phenol solution was placed in dark and stirred by a magnetic stirrer for 30 min

to achieve adsorption desorption equilibrium. The beaker was irradiated vertically in a solar system (UVA CUBE 400, Dr Hönle AG UV Technology, Germany) equipped with a halogen lamp (model: SOL 500), which is simulated to the natural sunlight (1000 W m^{-2}). At definite time intervals, a 1 mL sample was withdrawn from the beaker and 1 mL double distilled water was inserted instead to keep the distance between the light source and meniscus of solution constant all over the experiment duration. Phenol concentration in the withdrawn samples was determined by a high-performance liquid chromatograph (HPLC, Agilent 1260, USA) equipped with an analytical column Zorbax reverse-phase C18 and a diode-array detector at 280 nm wavelength. Each point was measured in triplet and the average was recorded. The column temperature was kept at 25 °C during the analysis. Gradient elution was obtained using water (mobile phase A) and acetonitrile (mobile phase B). 75% A mobile phase was eluted for 1 min, and then decreased to 60% A for 2 min. The flow rate of the mobile phase was kept at 0.5 mL min^{-1}. The generation of redox reactive species by NiS_2 after solar irradiation excitation was inspected by 1 mmol ammonium oxalate (AO) as the hole (h^+) scavenger agent, 1 mmol *para*-benzoquinon (*p*-BQ) as the superoxide radical ($O_2^{\bullet -}$) scavenger and 1 mmol isopropyl alcohol (IPA) as the hydroxyl radical ($^{\bullet}OH$) scavenger.

Results and discussion

Structural and elemental composition properties

The XRD and Raman data for the as-prepared NiS_2 layer are presented in Fig. 2. The XRD pattern of the NiS_2 layer (Fig. 2(a)) show sharp and dominant characteristic peaks of the NiS_2 cubic structure (JCPDS card no. 00-011-0099),[45] with no additional peaks related to any other crystalline nickel compounds such as nickel oxide, nickel hydroxide and other phases of nickel sulfides, indicating the complete transformation of the $Ni(OH)_2$ phase to NiS_2 phase.[47–49] The XRD analysis well matched with reported studies in literature.[28,30,31,50] The average crystallite size (D) of the NiS_2 layer was calculated using the Scherrer–Debye formula (eqn (6)) for the (200) reflection plane.

$$D_{(hkl)} = \frac{k\lambda}{\beta_{(hkl)}\cos\theta} \quad (6)$$

where K is the Debye constant, λ is the X-ray wavelength, β is the line broadening at full width at half maximum of the diffraction peak, and θ is the Bragg's angle.[51] The calculated crystallite size of the NiS_2 layers was approximately 26 nm.

The surface Raman spectrum measured at room temperature of the NiS_2 layer (Fig. 2(b)) shows the dominant characteristic peaks of the NiS_2 phase.[20] The peaks at 279 and 476 cm^{-1} are assigned to E_g and A_g photons, respectively. The observed peaks shifted towards a lower frequency compared with the NiS_2 single crystal. The obtained spectrum shows no noticeable characteristic peaks related to possible secondary phases and is consistent with previous reports.[11,28]

In order to study the elemental compositions and electronic states of the nanoflake NiS_2 layer, X-ray photoelectron spectroscopy (XPS) measurements were performed in this study.

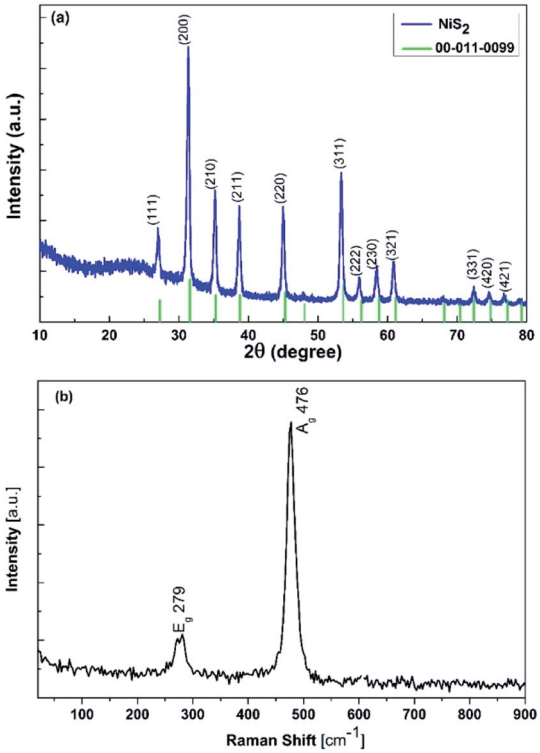

Fig. 2 (a) XRD pattern and (b) Raman spectrum of nanoflake NiS_2 layer.

Fig. 3(a) presents the high-resolution XPS spectrum of Ni 2p for the nanostructured NiS_2 layer, which has two main peaks appearing at 854.12 and 871.63 eV, fitting to the binding energy of Ni $2p_{3/2}$ and Ni $2p_{1/2}$, respectively. In addition, both Ni $2p_{3/2}$ and Ni $2p_{1/2}$ have shake-up satellite peaks located at 860.1 eV and 875.59 eV, respectively. Peak fitting analysis to separate overlapping peaks was made for the Ni $2p_{3/2}$ component, which indicates that it can be de-convoluted into a pair of peaks located at 854.12 and 856.05 eV, corresponding to Ni^{2+} and Ni^{3+} in NiS_2, respectively. The existence of Ni^{3+} results from the surface oxidation of NiS_2, which is in agreement with literature. The collected XPS results of the deconvolution of Ni 2p are in agreement with the reported binding energy values for Ni^{2+} and Ni^{3+}.[4,36] In addition, the spectral deconvolution of the S 2p spectrum (Fig. 3(b)) consists of two strong peaks at 162.91 (S $2p_{3/2}$) and 164.38 eV (S $2p_{1/2}$), implying the presence of unsaturated S atoms on the Ni–S and S–S bonds in NiS_2. These results fit well with NiS_2 single crystal XPS data.[22,29,52]

Morphological properties

The morphology of the NiS_2 layer was investigated by SEM. Fig. 4(a–d) shows the SEM images of the surface with different magnification, and cross section of the NiS_2 layer, synthesized on the glass substrate. The top view images of the as-prepared NiS_2 layer show that the surface of the NiS_2 sample reveals a rough nanoflake-like structure, with homogeneous and uniform distribution as well as a pinhole free layer. Moreover, the magnified view images show that the cross-linked nanoflakes are compact and uniform, resulting in a network

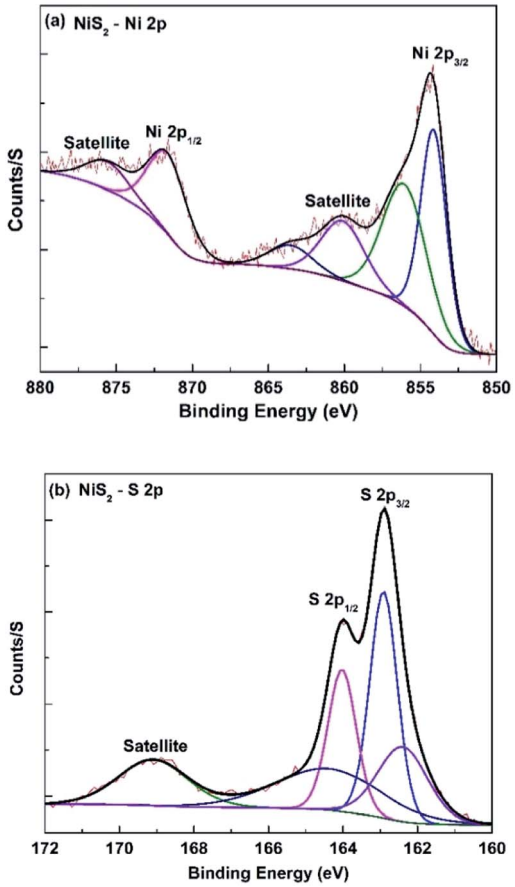

Fig. 3 XPS spectra of nanoflake NiS_2 layers: (a) Ni 2p and (b) S 2p.

architecture on the substrates. Also, the rough nanoflake edges observed clearly in Fig. 4(c) can be associated with the sulfurization process of the as-deposited $Ni(OH)_2$ layer as a result of gas release and dehydration during annealing, leading to the formation of NiS_2 with a high surface area structure.[44] The high surface area and rough morphology can significantly influence the photocatalytic performance of materials.[20,28] A cross-sectional image (Fig. 4(d)) exhibits that the NiS_2 layer has a uniform thickness in the range of approximately 950 nm.

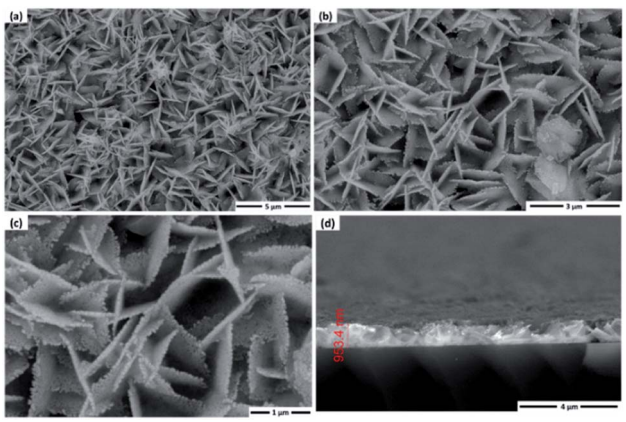

Fig. 4 (a–c) SEM images of NiS_2 with different magnifications, and (d) cross section of the NiS_2 layer.

Optical properties

The energy bandgap of NiS_2 was derived from the diffuse reflectance of the obtained layer using the Kubelka–Munk (KM) function[53,54], as indicated by the following equation:

$$F(R) = \frac{(1-R)^2}{2R} = \frac{\alpha}{S} \quad (7)$$

where $F(R)$ is the (KM) function, R is the diffused reflectance, α is the absorption coefficient, and S is the scattering coefficient. The optical band gap energy (E_g) of the NiS_2 layer can be calculated by the Tauc's equation:[55]

$$\alpha h\nu = A(h\nu - E_g)^n \quad (8)$$

where ($h\nu$) is the incident photon energy, α is the absorption coefficient, A is a constant, (E_g) is the optical band gap energy. Based on the KM function and Tauc's equation, the optical bandgap energy of the NiS_2 layer can be estimated using the following equation:

$$F(R)h\nu = A(h\nu - E_g)^n \quad (9)$$

The plots of $(F(R)h\nu)^2$ *vs.* $h\nu$ for indirect allowed transition are shown in Fig. 5. It was found that the estimated value of E_g for the NiS_2 layer was 1.19 eV, which is in agreement with reported values.[33,56] The low E_g value would allow the utilization of this material in photocatalytic applications under solar radiation.[29,57]

Photocatalytic activity measurements

The photocatalytic activity performance of the NiS_2 sample (5 cm^2) was examined using phenol as the model organic pollutant, two NiS_2 samples and at natural pH of 10 mg L^{-1} phenol. The variation of phenol relative concentration (C/C_0) is offered in Fig. 6 with the matching values of the 1st order apparent rate constants. Phenol presented insignificant

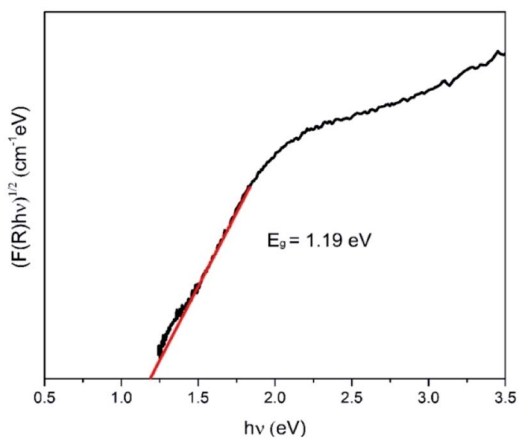

Fig. 5 $(F(R)h\nu)^{1/2}$ *vs.* $h\nu$ plot of the nanoflake NiS_2 layer.

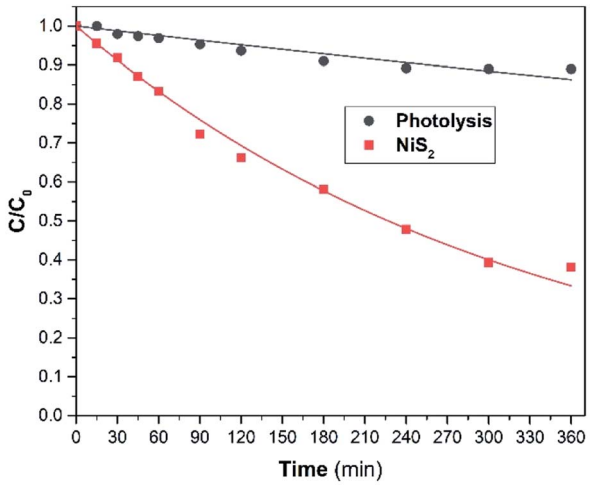

Fig. 6 Photocatalytic performance of NiS_2, phenol conc. = 10 mg L^{-1}, and natural pH 6.

photolysis under solar light. On the other hand, the rate of phenol photodegradation under solar light in the presence of the as-prepared NiS_2 layer was improved. This is due to the presence of the as-prepared NiS_2 slide, which absorbs solar light and photogenerates e^-/h^+ pairs utilized in photodegradation.

The main active species used in pollutant photodegradation are e^-, h^+, $^{\bullet}OH$ and $O_2^{\bullet-}$. The active species produced by NiS_2 are identified in Fig. 7. The active species identification was done by adding 1 mmol of each scavenger agent (AO, *p*-BQ and IPA) with 10 mg L^{-1} phenol and NiS_2 layer compared to the experiment done without any scavenger. As shown in Fig. 7, the primary active species is $O_2^{\bullet-}$ and h^+ is a secondary species, which are used as redox species in phenol photodegradation. Therefore, the proposed mechanism of the photocatalytic reactions is indicated by the following equations:

$$NiS_2 + h\nu \rightarrow NiS_2(h^+, e^-) \quad (10)$$

$$NiS_2(e^-) + O_2 \rightarrow NiS_2 + O_2^{\bullet-} \quad (11)$$

$$O_2^{\bullet-} + h^+ + \text{phenol} \rightarrow \text{photodegradation product} \quad (12)$$

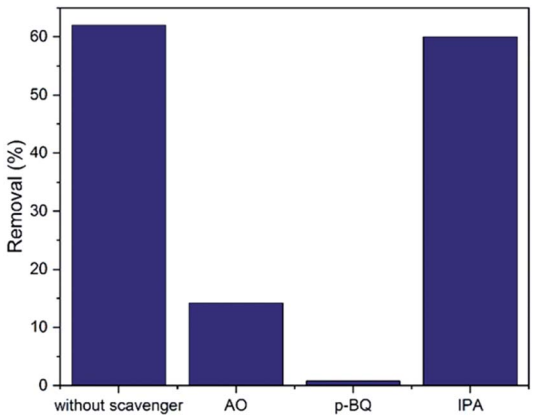

Fig. 7 Effect of scavengers on phenol removal efficiency.

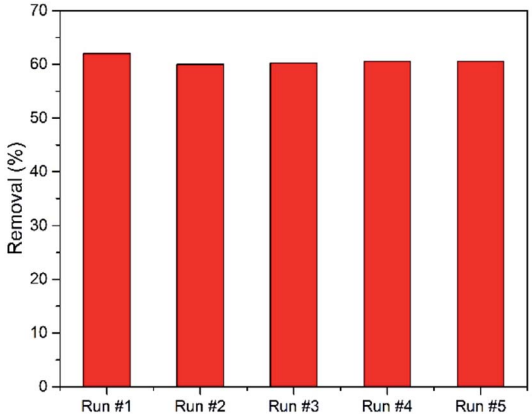

Fig. 8 Reusability of NiS_2, phenol conc. = 10 mg L^{-1}, and natural pH 6.

On the other hand, the NiS_2 reusability process is a very important issue, making the treatment process more economical. Fig. 8 shows a five cycle reusability test for NiS_2 phenol photodegradation. The removal efficiency was slightly decreased after the first cycle. Thereafter, there was no change in the phenol removal efficiency after each cycle.

Conclusion

A NiS_2 layer with a nanoflake-like structure was successfully synthesized by a facile two-step growth process. The $Ni(OH)_2$ layer was deposited on a glass substrate by chemical bath deposition, followed by a sulfurization process to obtain a single phase NiS_2 layer. The XRD and Raman analysis confirmed the formation of single-phase NiS_2. SEM revealed that the NiS_2 layer consisted of overlapping nanoflakes. XPS measurements revealed that the observed peaks from Ni 2p and S 2p spectra were attributed to NiS_2. The NiS_2 displayed a narrow optical bandgap of 1.19 eV. The NiS_2 nanoflake layer showed photocatalytic activity for the degradation of phenol under the irradiation of solar light at natural pH 6. The NiS_2 nanoflake layer exhibited good solar light photocatalytic degradation of phenol with good stability and reusability. The as-prepared NiS_2 layer can absorb solar irradiation and generate e^-/h^+ pairs. Hence, the NiS_2 layer is a promising photocatalyst for the photodegradation of destructive organic pollutants.

Author contributions

Mohammed M. Gomaa: conceptualization, data curation, formal analysis, investigation, methodology, writing – original draft. Mohamed H. Sayed: conceptualization, data curation, formal analysis, investigation, methodology, writing – original draft. Mahmoud S. Abdel-Wahed: conceptualization, methodology, data curation, formal analysis, investigation, writing – original draft. Mostafa Boshta: funding acquisition, project administration, resources, supervision, validation, writing – original draft.

Conflicts of interest

The authors declare no competing interests

Acknowledgements

The authors acknowledge the financial support from the National Research Centre Fund, through in-house projects number TT111001 and 12040110.

Notes and references

1 W. Zhu, Y. Cheng, C. Wang, N. Pinna and X. Lu, Transition metal sulfides meet electrospinning: versatile synthesis, distinct properties and prospective applications, *Nanoscale*, 2021, **13**, 9112.

2 G. An, L. Chenguang, Y. Hou, X. Zhang and Y. Liu, Transition metal dichalcogenide materials: solid-state reaction synthesis of nanocrystalline nickel disulfide, *Mater. Lett.*, 2008, **62**, 2643.

3 J. Li, P. Jiménez-Calvo, E. Paineau and M. N. Ghazzal, Metal chalcogenides based heterojunctions and novel nanostructures for photocatalytic hydrogen evolution, *Catalysts*, 2020, **10**, 89.

4 Y. Liang, Y. Yang, K. Xu, T. Yu, S. Yao, Q. Peng and C. Yuan, Crystal plane dependent electrocatalytic performance of NiS_2 nanocrystals for hydrogen evolution reaction, *J. Catal.*, 2020, **381**, 63.

5 C. H. Lai, M. Y. Lu and L. J. Chen, Metal sulfide nanostructures: synthesis, properties and applications in energy conversion and storage, *J. Mater. Chem.*, 2012, **22**, 19.

6 M. Dai and R. Wang, Synthesis and applications of nanostructured hollow transition metal chalcogenides, *Small*, 2021, **17**, 1.

7 B. T. Gadisa, R. Appiah-Ntiamoah and H. Kim, Amorphous iron sulfide nanowires as an efficient adsorbent for toxic dye effluents remediation, *Environ. Sci. Pollut. Res.*, 2019, **26**, 2734.

8 L. Peng, X. Ji, H. Wan, Y. Ruan, K. Xu, C. Chen, L. Miao and J. Jiang, Nickel sulfide nanoparticles synthesized by microwave-assisted method as promising supercapacitor electrodes: an experimental and computational study, *Electrochim. Acta*, 2015, **182**, 361.

9 J. Zhao, Y. Zhang, Y. Wang, H. Li and Y. Peng, The application of nanostructured transition metal sulfides as anodes for lithium ion batteries, *J. Energy Chem.*, 2018, **27**, 1536.

10 D. Mondal, G. Villemure, G. Li, C. Song, J. Zhang, R. Hui, J. Chen and C. Fairbridge, Synthesis, characterization and evaluation of unsupported porous NiS_2 sub-micrometer spheres as a potential hydrodesulfurization catalyst, *Appl. Catal., A*, 2013, **450**, 230.

11 Q. Ma, C. Hu, K. Liu, S. Hung, D. Ou and H. Ming, Nano energy identifying the electrocatalytic sites of nickel disulfide in alkaline hydrogen evolution reaction, *Nano Energy*, 2017, **41**, 148.

12 J. Wang, Z. Liu, C. Zhan, K. Zhang, X. Lai, J. Tu and Y. Cao, 3D hierarchical NiS_2/MoS_2 nanostructures on CFP with enhanced electrocatalytic activity for hydrogen evolution reaction, *J. Mater. Sci. Technol.*, 2020, **39**, 155.

13 A. Molla, M. Sahu and S. Hussain, Synthesis of tunable band gap semiconductor nickel sulphide nanoparticles: rapid and round the clock degradation of organic dyes, *Sci. Rep.*, 2016, **6**, 1.

14 X. Fang, T. Zhai, U. K. Gautam, L. Li, L. Wu, Y. Bando and D. Golberg, ZnS nanostructures: from synthesis to applications, *Prog. Mater. Sci.*, 2011, **56**, 175.

15 X. Chen, J. Zhang, J. Zeng, Y. Shi, S. Lin, G. Huang, H. Wang, Z. Kong, J. Xi and Z. Ji, MnS coupled with ultrathin MoS_2 nanolayers as heterojunction photocatalyst for high photocatalytic and photoelectrochemical activities, *J. Alloys Compd.*, 2019, **771**, 364.

16 P. Kumari, P. Chandran and S. S. Khan, Synthesis and characterization of silver sulfide nanoparticles for photocatalytic and antimicrobial applications, *J. Photochem. Photobiol., B*, 2014, **141**, 235.

17 D. Heift, Iron sulfide materials: catalysts for electrochemical hydrogen evolution, *Inorganics*, 2019, **7**, 75.

18 G. Ma, H. Peng, J. Mu, H. Huang, X. Zhou and Z. Lei, In situ intercalative polymerization of pyrrole in graphene analogue of MoS_2 as advanced electrode material in supercapacitor, *J. Power Sources*, 2013, **229**, 72.

19 J. Rakspun, N. Kantip, V. Vailikhit, S. Choopun and A. Tubtimtae, Multi-phase structures of boron-doped copper tin sulfide nanoparticles synthesized by chemical bath deposition for optoelectronic devices, *J. Phys. Chem. Solids*, 2018, **115**, 103.

20 C. Dai, B. Li, J. Li, B. Zhao, R. Wu, H. Ma and X. Duan, Controllable synthesis of NiS and NiS_2 nanoplates by chemical vapor deposition, *Nano Res.*, 2020, **13**, 2506.

21 Y. Yang, H. Zhu, H. Meng, W. Ma, C. Wang, F. Ma and Z. Hu, Nickel foam-supported starfish-like $Ni(OH)_2$@CoS nanostructure with obvious core–shell heterogeneous interfaces for hybrid supercapacitors application, *J. Mater. Sci.*, 2021, **56**, 3280.

22 N. Jiang, Q. Tang, M. Sheng, B. You, D. E. Jiang and Y. Sun, Nickel sulfides for electrocatalytic hydrogen evolution under alkaline conditions: a case study of crystalline NiS, NiS_2, and Ni_3S_2 nanoparticles, *Catal. Sci. Technol.*, 2016, **6**, 1077.

23 D. Zhang, X. Zhou, K. Ye, Y. Li, C. Song, K. Cheng, D. Cao, G. Wang and Q. Li, Synthesis of honeycomb-like NiS_2/NiO nano-multiple materials for high performance supercapacitors, *Electrochim. Acta*, 2015, **173**, 209.

24 K. F. Ulbrich, E. N. Nishida, B. S. Souza and C. E. M. Campos, NiS_2-NiS nanocrystalline composite synthesized by mechanochemistry and its performance for methylene blue dye adsorption, *Mater. Chem. Phys.*, 2020, **252**, 123226.

25 Q. Pan, J. Xie, S. Liu, G. Cao, T. Zhu and X. Zhao, Facile one-pot synthesis of ultrathin NiS nanosheets anchored on graphene and the improved electrochemical Li-storage properties, *RSC Adv.*, 2013, **3**, 3899.

26 R. Akbarzadeh, H. Dehghani and F. Behnoudnia, Sodium thiosulfate-assisted synthesis of NiS_2 nanostructure by

using nickel(II)-salen precursor: optical and magnetic properties, *Dalton Trans.*, 2014, **43**, 16745.

27 Y. Guo, D. Guo, F. Ye, K. Wang and Z. Shi, Synthesis of lawn-like NiS_2 nanowires on carbon fiber paper as bifunctional electrode for water splitting, *Int. J. Hydrogen Energy*, 2017, **42**, 17038.

28 S. L. Yang, H. Bin Yao, M. R. Gao and S. H. Yu, Monodisperse cubic pyrite NiS_2 dodecahedrons and microspheres synthesized by a solvothermal process in a mixed solvent: thermal stability and magnetic properties, *CrystEngComm*, 2009, **11**, 1383.

29 R. Karthikeyan, D. Thangaraju, N. Prakash and Y. Hayakawa, Single-step synthesis and catalytic activity of structure-controlled nickel sulfide nanoparticles, *CrystEngComm*, 2015, **17**, 5431.

30 W. Chen, X. Zhang, L. E. Mo, Z. Feng, S. Chen, X. Zhang, Y. Zhang and L. Hu, Ligands induced NiS_2 quantum dots for synchronous high specific capacity and robust stability of advanced electrochemical energy storage, *Chem. Eng. J.*, 2019, **375**, 121981.

31 M. M. Rahman, J. Ahmed, A. M. Asiri, I. A. Siddiquey and M. A. Hasnat, Development of 4-methoxyphenol chemical sensor based on NiS_2-CNT nanocomposites, *J. Taiwan Inst. Chem. Eng.*, 2016, **64**, 157.

32 T. T. Vu, S. Park, J. Park, S. Kim, V. Mathew, M. H. Alfaruqi, K. H. Kim, Y. K. Sun, J. Y. Hwang and J. Kim, Investigation of superior sodium storage and reversible Na_2S conversion reactions in a porous NiS_2@C composite using: in operando X-ray diffraction, *J. Mater. Chem. A*, 2020, **8**, 24401.

33 A. M. Huerta-Flores, L. M. Torres-Martínez, E. Moctezuma, A. P. Singh and B. Wickman, Green synthesis of earth-abundant metal sulfides (FeS_2, CuS, and NiS_2) and their use as visible-light active photocatalysts for H_2 generation and dye removal, *J. Mater. Sci.: Mater. Electron.*, 2018, **29**, 11613.

34 X. Yang, L. Zhou, A. Feng, H. Tang, H. Zhang, Z. Ding, Y. Ma, M. Wu, S. Jin and G. Li, Synthesis of nickel sulfides of different phases for counter electrodes in dye-sensitized solar cells by a solvothermal method with different solvents, *J. Mater. Res.*, 2014, **29**, 935.

35 C. Buchmaier, M. Glänzer, A. Torvisco, P. Poelt, K. Wewerka, B. Kunert, K. Gatterer, G. Trimmel and T. Rath, Nickel sulfide thin films and nanocrystals synthesized from nickel xanthate precursors, *J. Mater. Sci.*, 2017, **52**, 10898.

36 M. Lu, N. Gao, X. J. Zhang and G. S. Wang, Reduced graphene oxide decorated with octahedral NiS_2/NiS nanocrystals: facile synthesis and tunable high frequency attenuation, *RSC Adv.*, 2019, **9**, 5550.

37 M. Arivazhagan, A. Shankar and G. Maduraiveeran, Hollow sphere nickel sulfide nanostructures-based enzyme mimic electrochemical sensor platform for lactic acid in human urine, *Microchim. Acta*, 2020, **187**, 468.

38 V. A. V. Schmachtenberg, G. Tontini, J. A. Koch, G. D. L. Semione and V. Drago, Low temperature solventless syntheses of nanocrystalline nickel sulfides with different sulfur sources, *J. Phys. Chem. Solids*, 2015, **87**, 253.

39 M. Kristl, B. Dojer, S. Gyergyek and J. Kristl, Synthesis of nickel and cobalt sulfide nanoparticles using a low cost sonochemical method, *Heliyon*, 2017, **3**, 1.

40 W. F. W. Zakaria, A. A. Jalil, N. S. Hassan, M. Ibrahim and M. S. Azami, Visible-light driven photodegradation of phenol over niobium oxide-loaded fibrous silica titania composite catalyst, *J. Chem. Technol. Biotechnol.*, 2020, **95**, 2638.

41 G. U. Rehman, M. Tahir, P. S. Goh, A. F. Ismail, A. Hafeez and I. U. Khan, Enhancing the photodegradation of phenol using Fe_3O_4/SiO_2 binary nanocomposite mediated by silane agent, *J. Phys. Chem. Solids*, 2021, **153**, 110022.

42 F. Tzompantzi, J. C. Castillo-Rodríguez, C. Tzompantzi-Flores, R. Pérez-Hernández, R. Gómez, C. E. Santolalla-Vargas, G. Che-Galicia and E. Ramos-Ramírez, Addition of SnO_2 over an oxygen deficient zirconium oxide (Zr_xO_y) and its catalytic evaluation for the photodegradation of phenol in water, *Catal. Today*, 2021, DOI: 10.1016/j.cattod.2021.07.027.

43 X. Chen, Q. Liu, T. Bai, W. Wang, F. He and M. Ye, Nickel and cobalt sulfide-based nanostructured materials for electrochemical energy storage devices, *Chem. Eng. J.*, 2021, **409**, 127237.

44 B. Ju, H. J. Song, G. H. Lee, M. C. Sung and D. W. Kim, Nickel disulfide nanosheet as promising cathode electrocatalyst for long-life lithium–oxygen batteries, *Energy Storage Mater.*, 2020, **24**, 594.

45 S. Surendran, K. V. Sankar, L. J. Berchmans and R. K. Selvan, Polyol synthesis of α-NiS particles and its physico-chemical properties, *Mater. Sci. Semicond. Process.*, 2015, **33**, 16.

46 M. M. Gomaa, M. Boshta, B. S. Farag and M. B. S. Osman, Structural and optical properties of nickel oxide thin films prepared by chemical bath deposition and by spray pyrolysis techniques, *J. Mater. Sci.: Mater. Electron.*, 2016, **27**, 711.

47 D. Xiong, W. Li and L. Liu, Vertically aligned porous Nickel(II) hydroxide nanosheets supported on carbon paper with long-term oxygen evolution performance, *Chem.–Asian J.*, 2017, **12**, 543.

48 S. R. Ede, S. Anantharaj, K. T. Kumaran, S. Mishra and S. Kundu, One step synthesis of Ni/$Ni(OH)_2$ nano sheets (NSs) and their application in asymmetric supercapacitors, *RSC Adv.*, 2017, **7**, 5898.

49 A. A. Kashale, A. V. Ghule and I. W. P. Chen, Active edge site exposed β-$Ni(OH)_2$ nanosheets on stainless steel mesh as a versatile electrocatalyst for the oxidation of urea, hydrazine, and water, *ChemCatChem*, 2021, **13**, 1165.

50 R. Bhardwaj, R. Jha and M. Bhushan, Improved electrocatalytic performance with enlarged surface area and reduced bandgap of caterpillar and cabbage-like nickel sulphide nanostructures, *Appl. Nanosci.*, 2020, **10**, 3757.

51 M. Hjiri, M. S. Aida and G. Neri, NO_2 selective sensor based on α-Fe_2O_3 nanoparticles synthesized via hydrothermal technique, *Sensors*, 2019, **19**, 167.

52 S. P. Lonkar, V. V. Pillai and S. M. Alhassan, Scalable solid-state synthesis of MoS_2-NiS_2/graphene nanohybrids as

bifunctional electrocatalysts for enhanced overall water splitting, *Adv. Mater.*, 2020, **1**, 794.

53 S. Sharma and N. Khare, Sensitization of narrow band gap Bi_2S_3 hierarchical nanostructures with polyaniline for its enhanced visible-light photocatalytic performance, *Colloid Polym. Sci.*, 2018, **296**, 1479.

54 M. Patel, A. Chavda, I. Mukhopadhyay, J. Kim and A. Ray, Nanostructured SnS with inherent anisotropic optical properties for high photoactivity, *Nanoscale*, 2016, **8**, 2293.

55 M. M. Gomaa, M. H. Sayed, E. Chikoidze, Y. Dumont and M. Boshta, V-doped ZnO diluted magnetic semiconductor prepared by chemical spray pyrolysis, *Mater. Sci. Semicond. Process.*, 2020, **109**, 104944.

56 J. S. Anand, R. K. M. Rajan and M. Z. B. Abdul Aziz, Electrosynthesized NiS_2 thin films and their optical and semiconductor studies, *Rep. Electrochem.*, 2013, **3**, 25.

57 C. Schuster, M. Gatti and A. Rubio, Electronic and magnetic properties of NiS_2, NiSSe and $NiSe_2$ by a combination of theoretical methods, *Eur. Phys. J. B*, 2012, **85**, 1.